Noise Control Characteristics of Synchrophasing, Part 1: Analytical Investigation

C.R. Fuller*

Virginia Polytechnic Institute and State University, Blacksburg, Virginia

The noise control characteristics of synchrophasing are investigated using a simplified model of an aircraft fuselage. The analysis presented includes directivity effects of the noise sources and solves the coupled motion between the interior and exterior acoustic fields and the shell vibrational response in closed form. The variation in sound pressure level at various locations inside the shell is studied for various synchrophase angles as well as the shell vibrational response and input power flow in order to uncover the principal mechanisms behind the transmission phenomena.

Nomenclature

a	= shell mean radius
C_f	= fluid free speed of propagation
C_L	= shell free speed of propagation
E	= Young's modulus
FL	= fluid loading term
h	= shell wall thickness
I	= intensity
I_{33}	= (3,3) element of inverse matrix
k_s^r	= radial wave number
k_{ns}	= axial wave number
K_p	= pressure integrand
ℓ	= source index number
L	= matrix term
n	= circumferential mode number
p_{ex}, p_i	= acoustic pressure of exterior and interior fields, respectively
$\bar{p}_p$	= spectral pressure due to monopole source
p_0	= pressure amplitude of monopole source
p^{nd}	= nondimensional acoustic pressure
P	= acoustic power
P^{nd}	= nondimensional acoustic power
r, θ, x	= cylindrical coordinates
r_p	= radial location of monopole source
R_ℓ	= radial location of dipole source component
S	= matrix source term
t	= time
u, v, w	= shell displacement vectors
$\bar{U}, \bar{V}, \bar{W}$	= shell spectral displacement amplitudes
W_n^{nd}	= nondimensional shell radial displacement amplitude
β	= shell thickness parameter
ϵ	= 2 if $n=0$; = 1 if $n>0$
ϵ_n	= 1 if $n=0$; = 2 if $n>0$
η_f	= fluid loss factor
η_s	= shell loss factor
θ_ℓ	= angular location of dipole source component
ν	= Poisson's ratio
ρ_f	= density of fluid field
ρ_s	= density of shell material
ϕ_ℓ	= phase lead of dipole source component
ϕ_s	= synchrophase angle
ω	= source frequency, rad/s
Ω	= nondimensional source frequency

Superscript

( )*	= complex conjugate

Introduction

IN the last few years, considerable interest has arisen over the use of advanced turbopropeller (ATP) engines in powering passenger aircraft. This interest is mainly due to the possibility of up to 25% saving in fuel consumption over existing turbofan engines. However, associated with the use of ATP engines are high acoustic levels at the propeller locations due to supersonic tip speeds. There is concern that due to these high source inputs, the interior noise levels of ATP-powered aircraft will be in excess of acceptable limits, particularly for commercial applications. A compounding problem is that the fundamental harmonic of the propeller noise is typically between 100 and 250 Hz and the long wavelengths at these frequencies tend to render sound absorptive techniques ineffective.

One method of noise control—synchrophasing—shows a great deal of promise in that sound levels in a test aircraft were reduced by up to 8 dB without the penalty of an increase in takeoff weight that passive means of noise control incur. Synchrophasing, as a means of noise control, involves setting the relative rotational phase of each propeller until the interior noise levels are at a minimum. Although it has been shown experimentally[1,2] that synchrophasing can be effective, there exists no analytical model of the method and, consequently, very little physical understanding of the suppression mechanism. For instance, one of the conclusions of Ref. 1 is that synchrophasing provides a significant reduction in energy flux at the fuselage exterior rather than a redistribution of energy in the cabin of a Lockheed P-3C. This result is surprising using the simple interference interpretation of previous workers.

The aim of this paper is to investigate analytically the characteristics of synchrophasing for reduction of airborne interior noise. It is shown that, by using a simplified model of an aircraft, the principal mechanisms behind the synchrophasing concept can be uncovered. For the analysis presented here, the aircraft fuselage is approximated by an infinite cylindrical shell with typical material and properties. This model is appropriate in the light of measurements which show that vibration levels on a typical aircraft fuselage decay with distance away from the propeller plane.[1] The acoustic sources of each propeller (in this case, a twin-engine aircraft) are modeled by dipoles located at the source locations of typical propeller-driven aircraft. The advantage of using dipole sources is that the directionality and strength of each source can be adjusted to approximate actual pressure distributions at the fuselage. In other words, this arrangement effectively overcomes the need for complicated propeller radiation theory in the analysis.

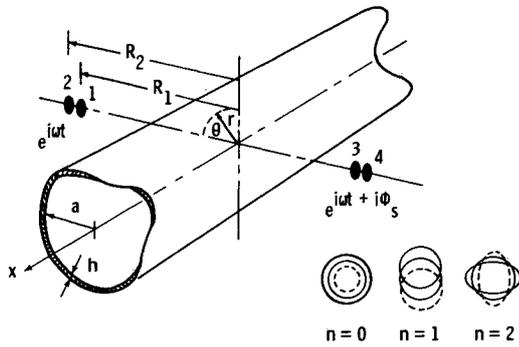*Associate Professor, Department of Mechanical Engineering.

Fig. 1 Geometry, coordinate system, and model shapes.

The acoustic response of the interior and exterior fields of the shell can then be obtained by writing the shell response in spectral form with forcing functions due to the dipole sources. These parameters are examined for various phase differences between the dipole sources corresponding to the synchrophasing concept. In addition, the radial intensity and line power flow into the shell are evaluated at the shell wall.

Analysis

The cylindrical coordinate system and the geometry employed in the analysis are shown in Fig. 1. Also shown are the first three circumferential mode shapes of the shell response. The method of analysis will be, first, to derive the response of the system for one monopole source. The response of the complete system will then be outlined, based on linear superposition, by addition of the response of each monopole source with the appropriate phases, amplitudes, and locations.

The Monopole Source

To obtain the vibrational response of the system shown in Fig. 1 to a monopole source located at $r = r_p$, $\theta = 0$, and $x = 0$ it is convenient to express the shell displacements as Fourier transforms,[3] viz.,

$$u = (1/\sqrt{2\pi}) \sum_{n=0}^{\infty} \cos(n\theta) \int_{-\infty}^{\infty} \bar{U}_n \exp(ik_{ns}x - i\omega t + i\pi/2) \mathrm{d}k_{ns}$$

(1a)

$$v = (1/\sqrt{2\pi}) \sum_{n=0}^{\infty} \sin(n\theta) \int_{-\infty}^{\infty} \bar{V}_n \exp(ik_{ns}x - i\omega t) \mathrm{d}k_{ns}$$

(1b)

$$w = (1/\sqrt{2\pi}) \sum_{n=0}^{\infty} \cos(n\theta) \int_{-\infty}^{\infty} \bar{W}_n \exp(ik_{ns}x - i\omega t) \mathrm{d}k_{ns}$$

(1c)

and, similarly, the associated interior acoustic field is

$$p_i = (\omega^2 \rho_f / \sqrt{2\pi}) \sum_{n=0}^{\infty} \cos(n\theta) \int_{-\infty}^{\infty} \bar{W}_n [J_n(k_s^r a)/J_n'(k_s^r a)k_s^r a]$$

$$\times \exp(ik_{ns} - i\omega t) \mathrm{d}k_{ns}$$

(2)

The pressure field at the shell wall, $r = a$, associated with an exterior monopole source has been previously derived by James[4] and, written in spectral form, is

$$\bar{p}_p = -(2/\sqrt{2\pi}) p_0 \epsilon_n H_n(k_s^r r_p)/H_n'(k_s^r a)k_s^r a$$

$$+ \rho_f \omega^2 \bar{W}_n H_n(k_s^r a)/H_n'(k_s^r a)k_s^r a$$

(3)

where the monopole amplitude p_0 has the units of force per unit length. The radial wave number k_s^r will be defined shortly.

Substitution of Eqs. (1-3) into the equations of motion of the fluid-loaded shell previously derived in Ref. 3 gives the spectral equations of motion of the forced displacement response of the system to the monopole source,

$$\begin{bmatrix} L_{11} & L_{12} & L_{13} \\ L_{21} & L_{22} & L_{23} \\ L_{31} & L_{32} & L_{33} \end{bmatrix} \begin{bmatrix} \bar{U}_n \\ \bar{V}_n \\ \bar{W}_n \end{bmatrix} = \begin{bmatrix} 0 \\ 0 \\ S_{31} \end{bmatrix}$$

(4)

where the elements of the matrix system are

$$L_{11} = -\Omega^2 + (k_{ns}a)^2 + \tfrac{1}{2}(1-\nu)n^2$$

(5a)

$$L_{12} = \tfrac{1}{2}(1+\nu)n(k_{ns}a)$$

(5b)

$$L_{13} = \nu(k_{ns}a)$$

(5c)

$$L_{21} = L_{12}$$

(5d)

$$L_{22} = -\Omega^2 + \tfrac{1}{2}(1-\nu)(k_{ns}a)^2 + n^2$$

(5e)

$$L_{23} = n$$

(5f)

$$L_{31} = L_{31}$$

(5g)

$$L_{32} = L_{23}$$

(5h)

$$L_{33} = -\Omega^2 + 1 + \beta^2[(k_{ns}a)^2 + n^2]^2 - \mathrm{FL}$$

(5i)

and the source term is given by

$$S_{31} = (2/\sqrt{2\pi}) \epsilon_n p_0 [H_n(k_s^r r_p)/H_n'(k_s^r a)k_s^r a] (\Omega^2/\rho_s \omega^2 h)$$

(6)

In Eqs. (5) and (6), Ω $(=\omega a/C_L)$ is the nondimensional frequency and β the thickness parameter given by $\beta^2 = h^2/12a^2$.

The fluid loading (FL) term due to the normal mode response of the contained fluid and the corresponding normal mode radiation pressure load is

$$\mathrm{FL} = \Omega^2(\rho_f/\rho_s)(h/a)^{-1}(k_s^r a)^{-1}[J_n(k_s^r a)/J_n'(k_s^r a)$$

$$- H_n(k_s^r a)/H_n'(k_s^r a)]$$

(7)

The nondimensional radial wave number can be obtained from the wave number-vector relationship

$$k_s^r a = \pm [\Omega^2(C_L/C_f)^2 - (k_{ns}a)^2]^{1/2}$$

(8)

Applying matrix theory to solve the system of Eq. (4) enables the spectral radial displacement amplitude to be written as

$$\bar{W}_n = (2/\sqrt{2\pi}) \epsilon_n p_0 [H_n(k_s^r r_p)/H_n'(k_s^r a)k_s^r a]$$

$$\times [\Omega^2/\rho_s \omega^2 h] I_{33}$$

(9)

where I_{33} is the (3,3) element of the inverse matrix L given by

$$I_{33} = (L_{11}L_{22} - L_{12}L_{21})/\det|L|$$

(10)

Application of the inverse transform of Eq. (1c) gives the radial displacement as

$$w(x/a,\theta) = p_0(\Omega^2/\pi\rho_s h a\omega^2) \sum_{n=0}^{\infty} \epsilon_n \cos(n\theta)$$

$$\times \int_{-\infty}^{\infty} [H_n(k_s^r r_p)/H_n'(k_s^r a)k_s^r a]$$

$$\times I_{33} \exp[i(k_{ns}a)(x/a)] \mathrm{d}(k_{ns}a)$$

(11)

Similarly, the inverse transform of Eq. (2) provides the interior acoustic pressure

$$p_i(r/a, x/a, \theta) = p_0(\Omega^2/\pi\rho_s ha\omega^2)\rho_f\omega a \sum_{n=0}^{\infty} \epsilon_n \cos(n\theta)$$

$$\times \int_{-\infty}^{\infty} [H_n(k_s^r r_p)/H_n'(k_s^r a)k_s^r a] [J_n(k_s^r r)/J_n'(k_s^r a)k_s^r a]$$

$$\times I_{33}\exp[i(k_{ns}a)(x/a)]d(k_{ns}a) \tag{12}$$

Likewise, the inverse transform of Eq. (3) provides the exterior acoustic pressure

$$p_{ex}(r/a, x/a, \theta) = -p_0(1/\pi a) \sum_{n=0}^{\infty} \epsilon_n \cos(n\theta)$$

$$\times \int_{-\infty}^{\infty} [H_n(k_s^r r_p)/H_n'(k_s^r a)k_s^r a]$$

$$\times \exp[i(k_{ns}a)(x/a)]d(k_{ns}a)$$

$$+ (\rho_f/\rho_s)\Omega^2(h/a)^{-1} \sum_{n=0}^{\infty} \epsilon_n \cos(n\theta)$$

$$\times \int_{-\infty}^{\infty} [H_n(k_s^r r_p)/H_n'(k_s^r a)k_s^r a]$$

$$\times [H_n(k_s^r r)/H_n'(k_s^r a)k_s^r a]I_{33}\exp[i(k_{ns}a)(x/a)]d(k_{ns}a)$$

$$\tag{13}$$

The Synchrophase Model

To investigate the characteristics of synchrophasing, the acoustic source at each propeller is modeled by a dipole. The synchrophase angle then corresponds to the phase difference between the dipole sources. The dipoles are constructed from two monopole sources located a small distance apart. The complete arrangement is shown in Fig. 1.

The response of the system, based on linearity, can then be considered as a superposition of the system's response to each monopole source. Thus, the total interior acoustic pressure for the system shown in Fig. 1 is

$$p_{total}/(p_{01}/a)(\rho_f/\rho_s)\Omega^2(h/a)^{-1}(1/\pi) = \exp[i\phi_1]$$

$$\times \sum_{n=0}^{\infty} \epsilon_n \cos(n\theta)\int_{-\infty}^{\infty} K_p(x/a, R_1)d(k_{ns}a)$$

$$+ (p_{02}/p_{01})\exp[i\phi_2] \sum_{n=0}^{\infty} \epsilon_n \cos(n\theta - n\theta_2)$$

$$\times \int_{-\infty}^{\infty} K_p(x/a, R_2)d(k_{ns}a)$$

$$+ (p_{03}/p_{01})\exp[i\phi_3]$$

$$\times \sum_{n=0}^{\infty} \epsilon_n \cos(n\theta - n\theta_3)\int_{-\infty}^{\infty} K_p(x/a, R_3)d(k_{ns}a)$$

$$+ (p_{04}/p_{01})\exp[i\phi_4] \sum_{n=0}^{\infty} \epsilon_n \cos(n\theta - n\theta_4)$$

$$\times \int_{-\infty}^{\infty} K_p(x/a, R_4)d(k_{ns}a) \tag{14}$$

where the pressure integrand is

$$K_p(x/a, r_p, r) = [H_n(k_s^r r_p)/H_n'(k_s^r a)k_s^r a]$$

$$\times [J_n(k_s^r r)/J_n'(k_s^r a)k_s^r a]I_{33}\exp[i(k_{ns}a)(x/a)] \tag{15}$$

In Eq. (14) the monopole sources numbered 1, 2, 3, and 4 are located at (R_1,θ_1), (R_2,θ_2), (R_3,θ_3), and (R_4,θ_4), respectively, as shown in Fig. 1. The sources also vibrate with amplitude ratios (respective to source 1) of p_{02}/p_{01}, p_{03}/p_{01}, and p_{04}/p_{01} and phase angle leads of ϕ_1, ϕ_2, ϕ_3, and ϕ_4, respectively, where the subscripts refer to the source number. As the theory developed previously is for a monopole source located at $\theta = 0$, in order to obtain Eq. (14), it is necessary to apply an angular coordinate transformation to each individual source response function.

Thus the synchrophase angle ϕ_s is the phase difference between the dipoles, and is specified by

$$\phi_s = \phi_3 - \phi_1 \tag{16}$$

Similar relationships can be derived for the total exterior acoustic field and shell vibrational response.

Results

In order to evaluate the shell response, the interior and exterior acoustic fields, and related variables it is necessary to evaluate integrals similar to those in Eq. (14). The integrands in this equation are transcendental functions with poles and branch points either on or very close to the real axis of the complete $k_{ns}a$ plane. The most convenient method of solution is to numerically evaluate the inverse transform integrals along the real axis. To avoid the singularities located on the integral path, damping is introduced both into the shell material and the fluid field. This has the effect of shifting the poles and branch points of the real axis. Structural damping is introduced by replacing Young's modulus E by $E(1 - i\eta_s)$, where η_s is the loss factor of the shell material. Fluid damping is introduced by changing the free speed of propagation C_f of the fluid to $C_f(1 - i\eta_f)$, where η_f is the fluid loss factor. Small values of loss factor were chosen (typically $\eta_s = 0.02$ and $\eta_f = 0.001$) and were found to have an insignificant effect on the final result; their presence essentially conditions the integrands for numerical evaluation. The integral was evaluated using Simpson's rule on a CYBER computer located at NASA Langley Research Center. The mesh size was chosen to be fine (typically $\Delta k_{ns}a = 0.001$) in order to accurately evaluate the integrand function near the singularities. The integral was also truncated at a finite value of $\pm k_{ns}a$ determined so as to include all of the poles and branch points and such that the integrand contribution after the truncation point is small. This method of evaluation of the shell response integral is similar to that used by Liu.[5]

The following results were calculated for a representative aircraft situation similar to that investigated by Mixson et al.[6] The shell material was taken to be aluminum with a nondimensional wall thickness of $h/a = 0.001$. The propagation medium was assumed to be air. The material properties are given in Table 1. The sources at each propeller location were set as pure dipoles, thus $\phi_2 - \phi_1 = \phi_3 - \phi_4 = \pi$ and were located such that $\theta_1 = \theta_2 = 0$ and $\theta_3 = \theta_4 = \pi$ at a nondimensional radial distance of $R_1/a = R_3/a = 3.0$ and $R_2/a = R_4/a = 3.1$. The nondimensional frequencies investigated were chosen to be $\Omega = 0.2$ and 0.14 which, for example, correspond to frequencies of 219 and 153 Hz in a 150-cm-diam fuselage. It is in this frequency range that the first propeller harmonic usually occurs.

Sound Pressure Level Reduction

Figure 2 shows the nondimensional exterior acoustic pressure,

$$p_{ex} = (p_{01}/a)(1/\pi)\Omega^2(\rho_f/\rho_s)(h/a)^{-1}p^{nd} \tag{17}$$

calculated along an axial line on the exterior surface of the shell such that $\theta = 0$. The results of Fig. 2 are calculated for $\Omega = 0.2$ and two different synchrophase angles. The general shape of the axial pressure distribution is very similar to that

Table 1   Material properties

Material	Young's modulus, N/m², ×10¹⁰	Poisson's ratio	Density, kg/m³	Free wave speed, m/s
Aluminum	7.1	0.33	2700	5150
Air	—	—	1.2	343

measured on a typical aircraft fuselage by Mixson et al.,[6] with high levels in the propeller plane where $x/a = 0$. This result suggests that the source directivity effects introduced by using dipoles provide a reasonable model of actual propeller sources. Changing the synchrophase angle has little effect on the axial pressure distribution, and implies that the surface pressure field on each side of the shell is largely unaffected by the source on the opposite side of the shell. The effect is most likely due to the acoustic shadowing of the shell surface and the directional nature of the source.

The corresponding internal pressure distribution calculated at $r = a$, $\theta = 0$ is plotted in Fig. 3. Unlike the external pressure distribution, the internal pressure field is very sensitive to the synchrophase angle and falls markedly when $\phi_s = 180$ deg. This behavior illustrates that the interior sound field is directly coupled to the shell vibrational motion and, thus, is markedly affected by synchrophase angle. The insertion loss (or noise reduction) by the shell wall can be directly obtained from the results of Figs. 2 and 3 and is plotted in Fig. 4. As shown, a change in the synchrophase angle can cause a large change in the calculated insertion loss. In effect, when $\phi_s = 180$ deg, the insertion loss of the shell wall is overestimated due to the inclusion of synchrophasing effects. Thus, care must be taken when measuring insertion losses on actual aircraft to at least synchrophase the propellers, in order to stabilize the measured value.

Figures 5-7 show the predicted amount of reduction in sound pressure levels at various interior locations for differing synchrophase angles between the dipole sources. The results were derived using Eq. (14), and are presented so as to be normalized to the maximum sound pressure level obtained in each figure. Because the sound pressure levels for $r/a = 0$ are far less than for $r/a = 1.0$ and 0.5, the values on the centerline are plotted with a 30-dB offset in order to keep the figures compact.

The results of Fig. 5 are for $x/a = 0$, $\theta = 0$, $\Omega = 0.2$, and three different radial points, and thus represent sound pressure levels in the "propeller plane" of the interior. It can be seen that the sound levels at each point can be significantly reduced if the correct synchrophase angle is chosen consistent with previous results obtained in practice.[1] It is also apparent that, as the observation point moves toward the shell wall, the optimum synchrophase angle and degree of attention change. This behavior can be understood by considering the radial response of the shell wall. Each dipole source excites a series of circumferential modes in the shell, which, in turn, couple, via the momentum boundary condition, to the interior acoustic field. The acoustic pressure at points inside the shell thus consists of varying (with cylindrical coordinates) superposition of circumferential modes due to the spatial variation in amplitude of each mode. If one considers the dipole sources in phase (i.e., zero synchrophase angle), then all odd circumferential modes will be suppressed; however, if the dipole sources are 180 deg out of phase than all even modes are suppressed. For the results of Fig. 5, the dominant *acoustic* mode excited by one dipole source is the $n = 2$ mode with a significant contribution from either the $n = 1$ or $n = 3$ mode depending upon radial location. Hence, the optimum synchrophase angle will be close to 180 deg but will vary with location depending upon the modal composition of the acoustic field at that point. At $r/a = 0$ only the $m = 0$ mode is present; thus, the optimum synchrophase angle is exactly 180 deg and the degree of obtainable at-
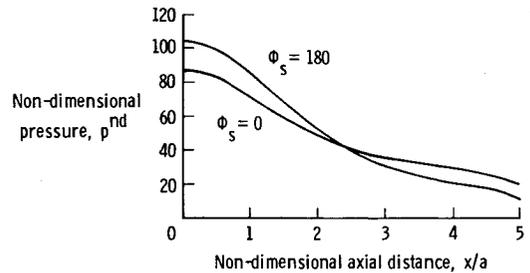

Fig. 2   Axial external pressure distribution: $r/a = 1$, $\theta = 0$, and $\Omega = 0.2$.
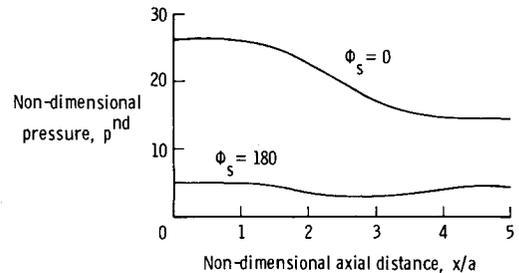

Fig. 3   Axial internal pressure distribution: $r/a = 1$, $\theta = 0$, and $\Omega = 0.2$.
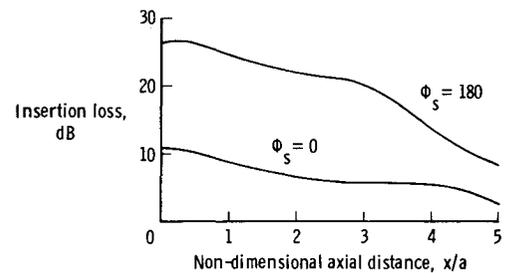

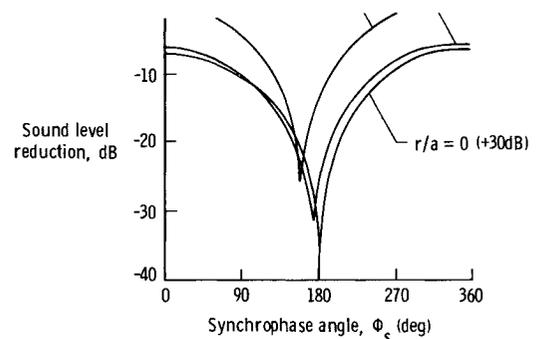**Fig. 4   Axial shell insertion loss:** $\theta = 0$ and $\Omega = 0.2$.

Fig. 5   Sound level reduction: $x/a = 0$, $\theta = 0$, and $\Omega = 0.2$.
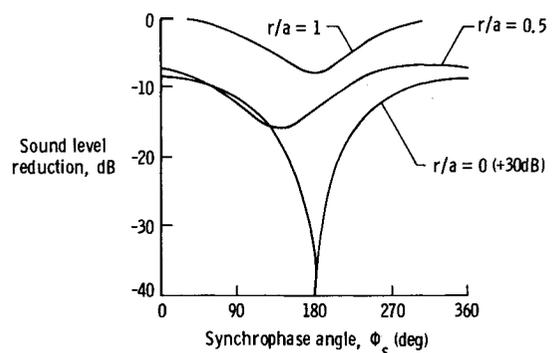

Fig. 6   Sound level reduction: $x/a = 10$, $\theta = 0$, and $\Omega = 0.2$.

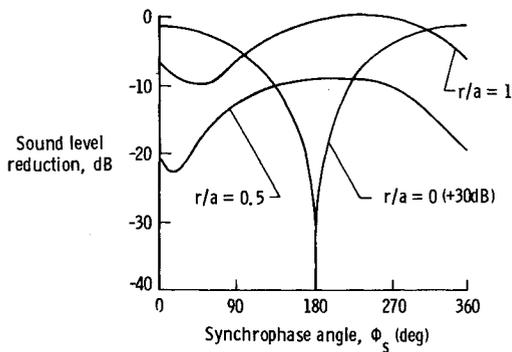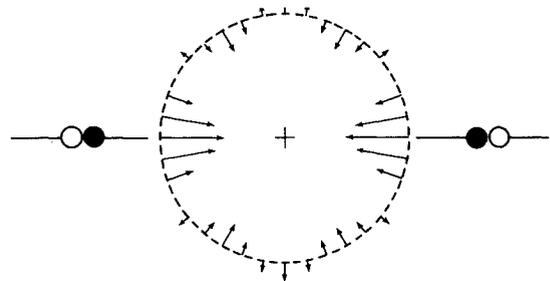Fig. 7 Sound level reduction: $x/a=0$, $\theta=0$, and $\Omega=0.14$.

Fig. 8 Normalized radial intensity at the shell wall: $x/a=0$, $\phi_s=0$ deg, and $\Omega=0.2$.

Fig. 9 Normalized radial intensity at the shell wall: $x/a=0$, $\phi_s=180$ deg, and $\Omega=0.2$.

tenuation (in decibels) is theoretically infinite at this location. At other radial locations the degree of attenuation obtained is finite for similiar reasons as just discussed.

Figure 6 presents synchrophase attenuation curves for $x/a=10$, $\theta=0$, and $\Omega=0.2$, and are thus at locations well out of the propeller plane and the associated near field of the sources. Again, at $r/a=0$, the optimum synchrophase angle is 180 deg. For differing radial locations the optimum synchrophase angle varies markedly, more so than at $x/a=0$. Similarly, the degree of attenuation available in the far field at differing radial locations can be seen to be far less than that obtained in the propeller plane (Fig. 5). Similar behavior was observed in synchrophasing experiments performed in a Lockheed P3-C.[1] The behavior was thought to be due to the acoustic modes having an axial variation in phase (due to differing phase velocities), as well as a spatial variation in amplitude. This increases the number of parameters to be optimized for sound reduction and consequently reduces the degree to which the sound levels can be minimized.

When the source frequency is changed to $\Omega=0.14$, the synchrophase attenuation curves presented in Fig. 7 are markedly different, except for $r/a=0$. The optimum synchrophase angle in this case is close to 0 deg; however, its actual value again varies from radial location. At a frequency of $\Omega=0.14$, the $n=1$ circumferential mode dominates the interior acoustic field and thus the optimum synchrophase angle is close to 0 deg. Hence, the optimum synchrophase angle also varies with frequency due to the changing modal response (or input mode impedance) of the system with frequency.

The results of Figs. 5-7 also show the relative radial variation in sound level in each case for a constant synchrophase angle. It is apparent that the highest levels obtained in all situations occur very close to the shell wall. Hence, this location would benefit the most from the application of synchrophasing. The levels calculated at the centerline are far lower than any of the other regions when $\phi_s \approx 0$, due to the predominant excitation of the $n=2$ mode which is null at $r/a=0$. Similarly, the results of Fig. 3 show that the internal acoustic pressure at $r=a$ falls quickly with x/a. Therefore, application of synchrophasing must also take into account the relative amplitude variation throughout the fuselage.

Radial Intensity and Power Flow at the Shell Wall

The radial intensity was calculated using the time-averaged intensity equation

$$I(x/a,\theta) = \tfrac{1}{2}Re[p \times (\dot{w})^*] \qquad (18)$$

The radial intensity vectors calculated at the shell wall are presented in Fig. 8, where $x/a=0$, $\Omega=0.2$, and the synchrophase angle is 0, i.e., the dipole sources are in phase. The magnitude of the intensity vector is normalized to the maximum value calculated. The intensity vectors demonstrate that, in the propeller plane when $\phi_s=0$, most of the acoustic energy enters through the shell in localized "hot spots" close to each source. This behavior is most likely due
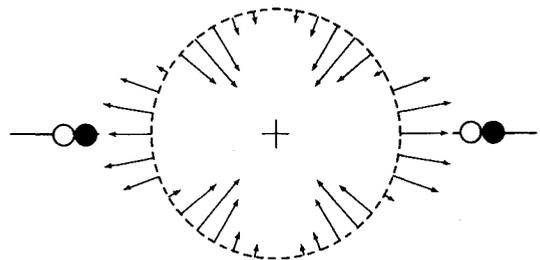
to the directional nature of the sources. What is surprising is that there are regions where acoustic energy *leaves* the shell near $\theta=\pi/2$ and $3\pi/2$.

When the synchrophase angle is changed to $\phi_s=180$ deg, the associated intensity vectors change dramatically (see Fig. 9). Now it can be seen that the acoustic energy enters the shell in regions close to $\theta=\pi/4$, $3\pi/4$, $5\pi/4$, and $7\pi/4$, and subsequently flows out of the shell in regions close to each source. The new power flow into the shell is still positive. To understand the physics of Fig. 9 it is necessary to remember that the intensity is time-averaged and thus, in real time, the vectors oscillate in magnitude. Thus, at the beginning of the harmonic cycle the energy flows from one dipole source, say, at $\theta=0$, through regions of the shell close to $\theta=\pi/4$ and $7\pi/4$ into the interior. Now, as the other source is 180 deg out of phase it acts as an acoustic sink and the acoustic energy then flows *out* of the shell close to $\theta=\pi$. As the harmonic cycle progresses, the situation reverses and the energy flows in the opposite direction. In other words, the presence of the dipole with a synchrophase angle of 180 deg causes the shell wall impedance in the source near field to fall markedly and thus sound can easily transmit through the wall in this region.

The line acoustic power flow (i.e., power flow per unit length of the shell) into the shell interior can be obtained by integrating the radial intensity at the shell wall with respect to $ad\theta$. Figure 10 presents the nondimensional line acoustic power such that

$$P = -P^{nd}(1/2\pi)(p_{01}/a)^2\Omega^4(\rho_f/\rho_s)(h/a)^{-2}\omega^{-1}\rho_s^{-1} \qquad (19)$$

at different locations along the wall axis for a synchrophase angle of $\phi_s=0$, and $\Omega=0.2$. The most interesting result in Fig. 10 is that it demonstrates that most of the acoustic energy (for one direction of propagation) enters the shell in a length equal to one shell diameter from the propeller plane. This localized flow of energy is due to the region of the shell surface being in the major lobe of the source radiation pattern where the forcing pressures are very high. It is also surprising to see that there is a length of shell immediately after the in-flow reigon where a significant amount of energy flows out of the shell. No reason for this behavior has been put forward thus far, but it was thought to be most likely due to radiation from that part of the shell vibrational near field that has long wavelengths.
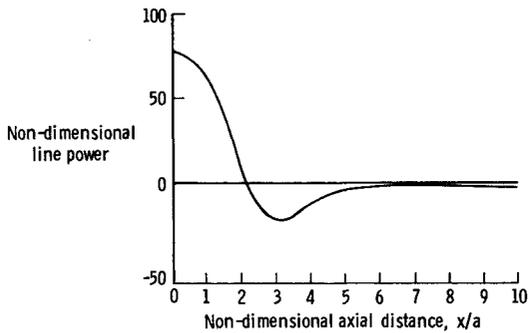
Fig. 10 Nondimensional line power flow at the shell wall: $\phi_s = 0$ deg and $\Omega = 0.2$.
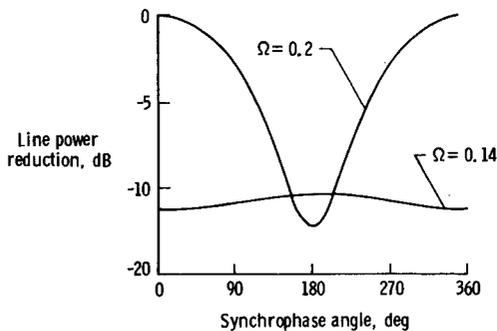

Fig. 11 Line power reduction at the shell wall: $x/a = 0$.

At large distances from the propeller plane the line power flow is much less but still out of the shell. Thus the acoustic energy enters the shell in a localized area centered on the propeller plane and then propagates as duct modes to locations away from the propeller plane. Because the shell has a high impedance relative to air, these duct modes propagate with only slight attenuation. However, at large values of x/a, the exterior acoustic field, due to direct radiation from the dipole sources, is small and, thus, the interior acoustic field energy radiates out to the external field via shell-coupled motion.

Figure 11 shows the calculated reduction in line power at the propeller plane for various synchrophasing angles for two frequencies: $\Omega = 0.2$ and 0.14. The optimum synchrophase angle for minimum input power flow for $\Omega = 0.2$ is close to 180 deg, indicating most of the power is carried by shell vibration in even circumferential modes. When the source frequency is changed to $\Omega = 0.14$, the optimum synchrophase angle is close to 0 deg because of the high response of the $n = 3$ mode. However, in this case, the net line power flow and the available reduction in line power are far less than for $\Omega = 0.2$.

Conclusions

An analysis has been presented by which the acoustic and structural response of a shell-fluid system excited by two dipole sources can be obtained in a closed-form solution. The arrangement is representative of a propeller-driven aircraft. The parameters of sound pressure level distribution, shell radial displacement amplitude, and energy flow into the interior have been evaluated for differing phase angles (i.e., the synchrophase effect) between the dipole sources. The results obtained have been used to investigate and explain the mechanisms behind the synchrophase effect. A number of important conclusions have been obtained:

1) Synchrophasing has been shown to theoretically provide significant sound level and shell vibration reduction.

2) The optimum synchrophase angle changes with interior location and frequency, and may be different for suppression of the interior acoustic field than suppression of the shell response or acoustic power flow into the shell. Thus, choice of the optimum synchrophase angle will ultimately depend upon a choice of one of the above criteria or a compromise between all of them.

3) The maximum achievable amount of attenuation of the interior acoustic field changes with location and frequency; however, it is greatest in the "propeller plane."

4) The three preceding conclusions are very similar to results actually measured in Lockheed P3-C[1], and thus serve to validate the model and its associated approximations presented in this paper.

5) Acoustic energy enters and leaves the shell in localized areas or "hot spots." The location of the hot spots changes dramatically with the synchrophase angle. This result tends to suggest the localized use of either acoustic or vibrational active control applied at the shell wall to obtain even greater sound or structural vibration attenuation. An alternative to active control may be the localized use of passive control methods. However, care must be taken to apply this only where energy enters the shell. Application in other areas may reduce sound attenuation.

6) The great majority of the acoustic energy enters the interior of the shell in a length of one shell diameter (for one direction of propagation) and propagates to other locations as interior duct modes. This implies that any form of additional noise control should be applied only in a fuselage diameter on either side of the propeller plane. A substantial amount of energy was found to flow out of the shell in a region located greater than one diameter from the propeller plane. It may be possible to enhance this effect for interior sound control away from the propeller plane.

7) The shell response is fundamental to the transmission mechanism due to its circumferential standing wave response and associated coupling behavior with the contained acoustic field. Thus, models for noise transmission into aircraft fuselages based on flat or finite curved plates are inadequate for low frequencies. Similarly, models based on random or plane wave incidence of sound, in which there are no source directivity characteristics (i.e., similar to architectural acoustics), are very likely to lead to spurious results.

Acknowledgments

References

[1]Johnston, J. L., Donham, R. E., and Guinn, W. A., "Propeller Signatures and Their Use," AIAA Paper 80-1035, 1980.

[2]Magliozzi, B., "Synchrophasing for Cabin Noise Reduction of Propeller-Driven Aircraft," AIAA Paper 83-0717, 1983.

[3]Fuller, C. R., "The Input Mobility of an Infinite Circular Cylindrical Elastic Shell Filled with Fluid," Journal of Sound and Vibration, Vol. 87, No. 3, 1983, pp. 409-427.

[4]James, J. H., "Computations of Acoustic Power, Vibration Response and Acoustic Pressures of Fluid-Filled Pipes," Admiralty Marine Technology Establishment, U.K., TM 82036, 1982.

[5]Lui, Y. N., personal communication, David W. Taylor Naval Ship Research and Development Center, Bethesda, MD, Nov. 1983.

[6]Mixson, J. S., Barton, C. K., Piersol, A. G., and Wilby, J. F., "Characteristics of Propeller Noise on an Aircraft Fuselage Related to Interior Noise Transmission," AIAA Paper 79-0646, 1979.